Circular Dichroism of Helicenes Investigated by Time-Dependent Density Functional Theory

Filipp Furche,[†] Reinhart Ahlrichs,*[,†] Claudia Wachsmann,[‡] Edwin Weber,[‡] Adam Sobanski,[§] Fritz Vögtle,[§] and Stefan Grimme[||]

Contribution from the Institut für Physikalische Chemie, Lehrstuhl für Theoretische Chemie, Universität Karlsruhe, Kaiserstrasse 12, 76128 Karlsruhe, Germany, Institut für Organische Chemie, TU Bergakademie Freiberg, Leipziger Strasse 29, 09596 Freiberg, Germany, Kekulé Institut für Organische Chemie und Biochemie, Universität Bonn, Gerhard-Domagk-Strasse 1, 53121 Bonn, Germany, and Institut für Physikalische und Theoretische Chemie, Universität Bonn, Wegelerstrasse 12, 53115 Bonn, Germany

Received June 11, 1999. Revised Manuscript Received November 29, 1999

Abstract: It is shown that molecular electronic circular dichroism (CD) can systematically be investigated by means of adiabatic time-dependent density functional theory (TDDFT). We briefly summarize the theory and outline its extension for the calculation of rotatory strengths. A new, efficient algorithm has been implemented in the TURBOMOLE program package for the present work, making large-scale applications feasible. The study of circular dichroism in helicenes has played a crucial role in the understanding of molecular optical activity. We present the first ab initio simulation of electronic CD spectra of [*n*]helicenes, $n = 4-7, 12$. Substituent effects are considered for the 2,15-dicyano and 2,15-dimethoxy derivates of hexahelicene; experimental CD spectra of these compounds were newly recorded for the present work. The calculations correctly reproduce the most important spectral features and greatly facilitate interpretation. We propose assignments of the low-energy bands in terms of individual excited states. Changes in the observed spectra depending on the number of rings and substitution patterns are worked out and rationalized. Merits and limitations of TDDFT in chemical applications are discussed.

I. Introduction

The chiroptical properties of a substance and its molecular structure are connected in a complicated and by no means obvious way. The desire to understand this relation has been a powerful stimulant to molecular structure theory from the very beginning, since optical activity is of considerable importance in organic chemistry and biochemistry but also in structural chemistry and materials science. In fact, there are hardly any other fields where simple models such as van't Hoff's asymmetric carbon atom, the electron on a helix,[1] or the octant rule for ketones[2] have been more successful to rationalize experiments. However, despite their usefulness, the scope of these models is limited because either they do not permit quantitative predictions or their validity is questionable. The same comment applies to semiempirical theories, although to a lesser extent. On the other hand, most traditional ab initio methods are still too expensive for applications to larger systems, or they suffer from approximations such as the neglect of electron correlation effects; in addition, an appealing physical interpretation is often difficult.

Time-dependent density functional theory (TDDFT)[3−6] has become an important tool for the theoretical treatment of molecular electronic excitation spectra.[7−10] Its success is rooted in a compromise between accuracy and computational efficiency. The theory has a simple, intuitive structure, since it uses the single-particle density as basic variable, which is directly observable. The price for this drastic simplification is that the total energy (or action in the time-dependent case) as a functional of the density is unknown and has to be approximated in practice.

In the present work we demonstrate the use of TDDFT for investigations of molecular electronic circular dichroism (CD).[11] In section II, we summarize the theory and extend it for the calculation of rotatory strengths which are required, besides the excitation energies, for the simulation of CD spectra. The formulation provides an intuitive picture in terms of occupied and virtual molecular orbitals (MOs). In section III, an outline of the new TURBOMOLE[12] TDDFT implementation is given. Although we will not go into details, we note that the applications presented here would not have been possible without this development.

The helicenes are model compounds for screw-shaped molecular systems which are important in nucleic acid, peptide,

* Author to whom correspondence should be addressed. E-mail: ramail@tchibm3.chemie.uni-karlsruhe.de.
[†] Universität Karlsruhe.
[‡] TU Bergakademie Freiberg.
[§] Kekulé Institut für Organische Chemie und Biochemie.
[||] Institut für Physikalische und Theoretische Chemie.

(1) Tinoco, I., Jr.; Woody, R. W. *J. Chem. Phys.* **1964**, *40*, 160.
(2) Moffit, W.; Woodward, R. B.; Moscowitz, A.; Klyne, W.; Djerassi, C. *J. Am. Chem. Soc.* **1961**, *83*, 4013.
(3) Runge, E.; Gross, E. K. U. *Phys. Rev. Lett.* **1984**, *52*, 997.
(4) Gross, E. K. U.; Kohn, W. *Adv. Quantum Chem.* **1990**, *21*, 255.
(5) Casida, M. E. Time-Dependent Density Functional Response Theory for Molecules. In *Recent advances in density functional methods*; Chong, D. P., Ed.; World Scientific: Singapore, 1995; Vol. 1.
(6) Gross, E. K. U.; Dobson, J. F.; Petersilka, M. *Top. Curr. Chem.* **1996**, *181*, 81.
(7) Bauernschmitt, R.; Ahlrichs, R. *Chem. Phys. Lett.* **1996**, *256*, 454.
(8) Jamorski, C.; Casida, M. E.; Salahub, D. R. *J. Chem. Phys.* **1996**, *104*, 5134.
(9) Görling, A.; Heinze, H. H.; Ruzankin, S. P.; Staufer, M.; Rösch, N. *J. Chem. Phys.* **1999**, *110*, 2785.
(10) Hirata, S.; Head-Gordon, M. H. *Chem. Phys. Lett.* **1999**, *302*, 375.
(11) Nakanishi, K., Berova, N., Woody, R. W., Eds. *Circular Dichroism: Principles and Applications*; VCH: New York, 1994.
(12) Ahlrichs, R.; Bär, M.; Häser, M.; Horn, H.; Kölmel, C. *Chem. Phys. Lett.* **1989**, *162*, 165 (current version: see http://www.chemie.uni-karlsruhe.de/PC/TheoChem).

10.1021/ja991960s CCC: $19.00
Published on Web 02/15/2000

and sugar chemistry.[13−15] They exhibit unique chiroptical properties such as large circular dichroisms and optical rotations whose study has been crucial for the understanding of molecular optical activity. We consider the CD spectra of [*n*]helicenes with 4−7 and 12 condensed rings as well as the 2,15-disubstituted cyano and methoxy derivatives (R = CN or OCH_3 in Figure 1) of hexahelicene. This continues and extends previous theoretical work on penta-, hexa-, and a pyrrolohexahelicene based on an approximate version of TDDFT.[16] Experimental CD spectra are available for all compounds except tetra- and dodecahelicene; those of the substituted hexahelicenes were newly recorded for the present work. Details of the computations and the experimental conditions are given in section IV and V, respectively. The discussion of results in section VI starts with general considerations on the nature and classification of excited states in helicenes. Calculated spectra are compared in detail with experimental data for each compound; the lowest excited singlet states are reassigned. Special emphasis is placed on systematic trends and correlations between structure and properties. Finally, in section VII, we summarize our findings and discuss the potential of TDDFT for applications in chemistry.

II. Theory

The starting point for the calculation of electronic excitations within the adiabatic approximation of time-dependent density functional linear response theory[5,7,9,17] is the RPA-type[18] eigenvalue problem

$$\begin{pmatrix} A & B \\ B & A \end{pmatrix}\begin{pmatrix} X^{0n} \\ Y^{0n} \end{pmatrix} = \omega^{0n}\begin{pmatrix} 1 & 0 \\ 0 & -1 \end{pmatrix}\begin{pmatrix} X^{0n} \\ Y^{0n} \end{pmatrix} \tag{1}$$

with the normalization condition

$$X^{0n^T}X^{0n} - Y^{0n^T}Y^{0n} = 1 \tag{2}$$

for all positive ω^{0n}.[18] The vectors X^{0n} and Y^{0n} describe the electron−hole and hole−electron components of the excitation. For spin-restricted closed-shell systems, eq 1 separates into two distinct eigenvalue problems for singlet (*s*) and triplet (*t*) excitations.[7] In this case, the matrix elements of *A* and *B* read

$$(A_s - B_s)_{iajb} = (A_t - B_t)_{iajb} = (\epsilon_a - \epsilon_i)\delta_{ij}\delta_{ab} \tag{3}$$

$$(A_s + B_s)_{iajb} = (\epsilon_a - \epsilon_i)\delta_{ij}\delta_{ab} + 4\int \mathrm{d}^3r\, \mathrm{d}^3r'\, \frac{\varphi_a(\mathbf{r})\,\varphi_j(\mathbf{r}')\,\varphi_i(\mathbf{r})\,\varphi_b(\mathbf{r}')}{|\mathbf{r}-\mathbf{r}'|} + 2\int \mathrm{d}^3r\, \mathrm{d}^3r'\, \varphi_a(\mathbf{r})\,\varphi_j(\mathbf{r}')\,(f_{\mathrm{xc}\alpha\alpha}(\mathbf{r},\mathbf{r}') + f_{\mathrm{xc}\alpha\beta}(\mathbf{r},\mathbf{r}'))\,\varphi_i(\mathbf{r})\,\varphi_b(\mathbf{r}') \tag{4}$$

$$(A_t + B_t)_{iajb} = (\epsilon_a - \epsilon_i)\delta_{ij}\delta_{ab} + 2\int \mathrm{d}^3r\, \mathrm{d}^3r'\, \varphi_a(\mathbf{r})\,\varphi_j(\mathbf{r}')\,(f_{\mathrm{xc}\alpha\alpha}(\mathbf{r},\mathbf{r}') - f_{\mathrm{xc}\alpha\beta}(\mathbf{r},\mathbf{r}'))\,\varphi_i(\mathbf{r})\,\varphi_b(\mathbf{r}') \tag{5}$$

The orbitals $\varphi_u(\mathbf{r})$ with eigenvalues ϵ_u are solutions of the closed-shell Kohn−Sham equations for the molecular ground state; as usual, *i*, *j*, ... denote occupied, *a*, *b*, ... virtual and *u*, *v*, ... general MOs. $f_{\mathrm{xc}\sigma\sigma'}(\mathbf{r},\mathbf{r}')$ is the static exchange-correlation kernel,

$$f_{\mathrm{xc}\sigma\sigma'}(\mathbf{r},\mathbf{r}') = \frac{\delta^2 E_{\mathrm{xc}}}{\delta\rho_\sigma(\mathbf{r})\,\delta\rho_{\sigma'}(\mathbf{r}')} \tag{6}$$

Explicit expressions for the A and B matrix elements using approximations to the exchange-correlation functional E_{xc} which are local in the density and its gradients are given in ref 7. We use atomic (Hartree) units throughout, unless otherwise stated.

In the TDDFT framework, the eigenvalues ω^{0n} are interpreted as excitation energies of the interacting system. Moreover, transition densities $\rho^{0n}(\mathbf{r})$ and transition current densities $\mathbf{j}^{0n}(\mathbf{r})$ of singlet excitations are given by

$$\rho^{0n}(\mathbf{r}) = \sqrt{2}\sum_{i,a}(X+Y)_{ia}^{0n}\,\varphi_i(\mathbf{r})\,\varphi_a(\mathbf{r}) \qquad \text{and}$$

$$\mathbf{j}^{0n}(\mathbf{r}) = \frac{\sqrt{2}}{2}\sum_{i,a}(X-Y)_{ia}^{0n}(\varphi_a(\mathbf{r})\,\boldsymbol{\pi}\varphi_i(\mathbf{r}) + \varphi_i(\mathbf{r})(\boldsymbol{\pi}\varphi_a(\mathbf{r}))^*) \tag{7}$$

$\boldsymbol{\pi}$ is the kinematical momentum operator. This nontrivial statement follows from the observation[6] that the densities *and* the current densities of the time-dependent interacting and Kohn−Sham systems are identical. It considerably enlarges the applicability range of TDDFT, making chiroptical properties such as rotatory strengths accessible.

$\rho^{0n}(\mathbf{r})$ and $\mathbf{j}^{0n}(\mathbf{r})$ are the changes in charge and current density associated with the *n*th excitation from the ground state. Thus, the electric transition dipole moment $\boldsymbol{\mu}^{0n}$ is given by

$$\boldsymbol{\mu}_l^{0n} = -\int \mathrm{d}^3r\, \rho^{0n}(\mathbf{r})\,\mathbf{r} \tag{8}$$

in the dipole-length form and

$$\boldsymbol{\mu}_v^{0n} = \frac{1}{\mathrm{i}\omega^{0n}}\int \mathrm{d}^3r\, \mathbf{j}^{0n}(\mathbf{r}) \tag{9}$$

in the dipole-velocity form.[19] Both formulations are identical in a complete basis, as can be most easily shown by means of the continuity equation[20]

$$\mathrm{i}\omega^{0n}\rho^{0n}(\mathbf{r}) = \nabla\mathbf{j}^{0n}(\mathbf{r}) \tag{10}$$

which is valid independently of approximations to E_{xc}. In finite basis sets, though, eq 10 is generally not obeyed and the length and velocity forms differ. Alternatively, gauge invariance[21] can be invoked to demonstrate the equivalence of both formulations. The magnetic transition dipole moments $\mathbf{m}^{0n}$ are calculated from

$$\mathbf{m}^{0n} = \frac{1}{2c}\int \mathrm{d}^3r\, \mathbf{r}\times\mathbf{j}^{0n}(\mathbf{r}) \tag{11}$$

Measurable quantities such as singlet oscillator strengths f^{0n} and rotatory strengths R^{0n} are related to the transition dipole moments by

$$f^{0n} = \frac{2}{3}\omega^{0n}|\boldsymbol{\mu}^{0n}|^2 \tag{12}$$

and

(13) Meurer, K. P.; Vögtle, F. *Top. Curr. Chem.* **1985**, *127*, 1.
(14) Martin, R. H. *Angew. Chem., Int. Ed. Engl.* **1974**, *13*, 649.
(15) Laarhoven, H.; Prinsen, J. C. *Top. Curr. Chem.* **1983**, *125*, 63.
(16) Grimme, S.; Harren, J.; Sobanski, A.; Vögtle, F. *Eur. J. Org. Chem.* **1998**, 1491.
(17) Petersilka, M.; Grossmann, U. J.; Gross, E. K. U. *Phys. Rev. Lett.* **1996**, *76*, 1212.
(18) McLachlan, A. D.; Ball, M. A. *Rev. Mod. Phys.* **1964**, *36*, 844.
(19) Hansen, A. E.; Bouman, T. D. *Adv. Chem. Phys.* **1980**, *44*, 545.
(20) Furche, F.; Ahlrichs, R. In preparation.
(21) Goeppert-Mayer, M. *Ann. Phys.* **1931**, *9*, 273.

$$R^{0n} = \mathrm{Im}(\boldsymbol{\mu}^{0n} \cdot \mathbf{m}^{0n*}) \tag{13}$$

It is convenient to introduce

$$Z^{0n} = \sqrt{\omega^{0n}}(A - B)^{-1/2}(X^{0n} + Y^{0n}) \tag{14}$$

which is a solution of the *symmetric* eigenvalue problem

$$(A - B)^{1/2}(A + B)(A - B)^{1/2}Z^{0n} = (\omega^{0n})^2 Z^{0n} \tag{15}$$

of half the dimension of problem 1.[7] We suppress spin indices *s*, *t* here for simplicity. The vectors Z^{0n} are normalized to unity in the sense

$$||Z^{0n}||^2 = \sum_{i,a} |Z_{ia}^{0n}|^2 = 1 \tag{16}$$

Thus, the coefficients $|Z_{ia}^{0n}|^2$ give the relative weight of the single-particle excitation from occupied orbital $\varphi_i(\mathbf{r})$ to virtual orbital $\varphi_a(\mathbf{r})$ in the transition described by Z^{0n}. This is useful for assignment and interpretation.

The neglect of the frequency dependence of f_{xc} in eq 6 is known as the "adiabatic approximation".[4,22] Recently, Baerends et al.[23] have suggested that, in the low-frequency regime, the error resulting from the adiabatic approximation is small compared to the error emerging from local approximations to the static exchange-correlation functional E_{xc}. In fact, there is enough evidence that excited states lying well below the Kohn−Sham continuum are properly described.[7,24] It is, however, a well-known deficiency of local and gradient-corrected functionals that they give Kohn−Sham ionization thresholds much lower than experimental ionization energies, whereas both should agree if the exact exchange-correlation functional were used.[25] Several ad hoc corrections have been suggested to remedy this shortcoming.[24,26]

III. Implementation

The simulation of CD spectra requires the solution of eigenvalue problem 15 for a relatively large number of electronic excitations. This has been newly implemented in the TURBOMOLE program package[12] for the present work. Thus, systems with more than 1000 basis functions without symmetry have become routinely tractable on workstation computers. In the following, we will only give a survey of the most important features.

The most efficient way to solve problem 15 is the direct iterative approach:[7,27] Matrix $M = (A - B)^{1/2}(A + B)(A - B)^{1/2}$ is never actually constructed, as only products of M with test vectors are required. Unlike in the HF-RPA case, the computation of $(A - B)^{1/2}$ and its inverse is trivial for TDDFT since $(A - B)$ is diagonal in a real orbital basis, eq 3. The multiplication of a vector by $(A + B)$ is the time-determining step; it is done most conveniently in the atomic orbital (AO) basis in an integral-direct fashion.[27] Due to its similarity with the ground-state Fock matrix construction, efficient integral evaluation and quadrature codes are available. If N measures the system size, the asymptotic scaling of computation time per matrix-vector-product in our implementation is proportional to N^2 for the Coulombic and nearly linear for the exchange-correlation part. The transformation formally scales as N^3; due to a very small factor, however, this is insignificant for systems with up to several thousand basis functions.

A crucial point in our approach is the simultaneous treatment of several excitations. We found the block Davidson algorithm in the formulation of Crouzeix et al.[28] most appropriate for the present problem. Compared with the single-vector method, the cost per eigenpair is substantially lowered, mainly as integral evaluation needs to be done only once for all vectors in every iteration, and convergence is much better. Even further savings without significant loss in accuracy can be achieved by auxiliary basis set expansion (RI) techniques;[5,9,29] preliminary results indicate that acceleration by about an order of magnitude is feasible.

We fully exploit molecular symmetry for all finite point groups. This is useful for assignment, since excitations normally are classified according to the irreducible representations (IRs) of the molecular point group G. Even more important, operation count is lowered by about a factor of 1/ord(G), and convergence is assisted. We use explicit Clebsch−Gordan reduction of the product space of occupied and virtual MOs, while skeleton operator techniques[30−32] are favorable for computations in the AO basis.

IV. Computational Details

A. Equilibrium Structures. The structures employed in the present work were optimized at the Hartree−Fock (HF) level of theory using a standard TURBOMOLE SV(P) basis set.[33] We will merely give a brief summary of results here and refer to the work of Grimme and Peyerimhoff[34] for a more detailed discussion.

In the larger compounds ($n > 4$), the C−C bond lengths vary between 135 and 146 pm; the pattern of bond length alternation closely resembles that of naphthalene or phenanthrene. The bond lengths obtained from X-ray structures of penta-, hexa- and heptahelicene[35−37] agree with the theoretical values to within 2−3 pm, which is below experimental accuracy. The surprising success of HF/SV(P) results from a well-known error compensation between the neglect of correlation and basis set truncation. In contrast, exploratory DFT calculations with GGA and hybrid functionals lead to inferior results. However, a detailed comparison with experiment is hampered by packing or disordering effects leading to nonsymmetrical structures.

Most important for the chirality of the helicenes is their helical shape as, e.g., measured by the dihedral angles of consecutive carbon atoms in the inner part (i.e., atoms without a number in Figure 1, e.g., for hexahelicene starting with C(1) and ending with C(16)). The computed angles increase from tetra- (18.6°) to pentahelicene (18.1° and 30.5°), decrease for hexahelicene (14.1° and 28.9°), and then remain approximately constant between 15° and 28° for the larger molecules. This indicates that the largest change in structure compared to usually planar aromatic hydrocarbons occurs between $n = 4$ and $n = 5$ (see also section VI). The shortest nonbonding C−C distances between "overlapping" rings are predicted to be 309 pm for hexa- and 304 pm for heptahelicene, which is close to twice the van der Waals radius of

(22) Zangwil, A.; Soven, P. *Phys. Rev. A* **1980**, *21*, 1561.
(23) van Gisbergen, S. J. A.; Kootstra, F.; Schipper, P. R. T.; Gritsenko, O. V.; Snijders, J. G.; Baerends, E. J. *Phys. Rev. A* **1998**, *57*, 2556.
(24) Casida, M. E.; Jamorski, C.; Casida, K. C.; Salahub, D. R. *J. Chem. Phys.* **1998**, *108*, 4439.
(25) van Leeuven, R.; Gritsenko, O. V.; Baerends, E. J. *Top. Curr. Chem.* **1995**, *180*, 107.
(26) Tozer, D. J.; Handy, N. C. *J. Chem. Phys.* **1998**, *109*, 10180.
(27) Weiss, H.; Ahlrichs, R.; Häser, M. *J. Chem. Phys.* **1993**, *99*, 1262.
(28) Crouzeix, M.; Philippe, B.; Sadkane, M. *SIAM J. Sci. Comput.* **1994**, *15*, 62.
(29) Bauernschmitt, R.; Häser, M.; Treutler, O.; Ahlrichs, R. *Chem. Phys. Lett.* **1997**, *264*, 573.
(30) Dupuis, M.; King, H. F. *Int. J. Quantum Chem.* **1977**, *11*, 613.
(31) Taylor, P. R. *Int. J. Quantum Chem.* **1985**, *27*, 89.
(32) van Wüllen, C. *Chem. Phys. Lett.* **1994**, *219*, 8.
(33) Schäfer, A.; Horn, H.; Ahlrichs, R. *J. Chem. Phys.* **1992**, *97*, 2571.
(34) Grimme, S.; Peyerimhoff, S. D. *Chem. Phys.* **1996**, *204*, 411.
(35) McIntosh, A. O.; Mouteath-Robertson, J.; Vaud, V. *J. Chem. Soc.* **1954**, 1661.
(36) DeRango, C.; Tsoucaris, G.; Delerq, J. P.; Germain, G.; Putzeys, J. P. *Cryst. Struct. Commun.* **1973**, *2*, 189.
(37) van den Hark, T. E. M.; Beurskens, P. T. *Cryst. Struct. Commun.* **1976**, *5*, 247.

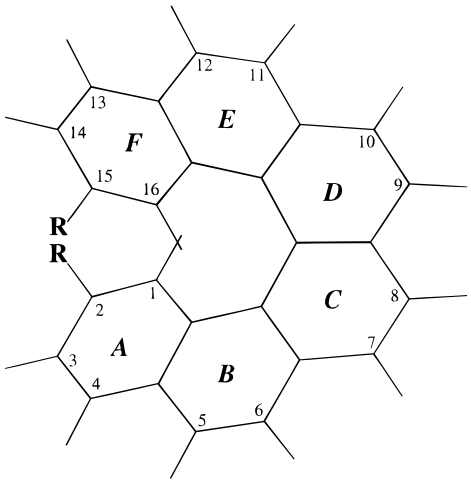

Figure 1. Structure of substituted hexahelicenes with atom and ring numbering.

carbon, but 3−4% larger than experimental results. The slight overestimation of the total helix height is not unexpected since attractive dispersion effects are neglected in the HF treatment.

The structures of 2,15-dicyanohexahelicene and its parent compound differ significantly. This is most obvious in the substituted terminal rings (a maximum change of 5 pm is calculated for the bonds C(2)−C(1) and C(2)−C(3)). All values for the C−C bond lengths of the dimethoxy derivate are within 1 pm of the corresponding values for the parent compound. The dihedral angles change by less than 0.5° upon substitution. Thus, substituent effects found in the CD spectra are expected to result mainly from changes in electronic rather than in geometric structure.

B. TDDFT Response Calculations. Singlet excitation energies and transition moments of the (M)-enantiomers in both irreducible representations of the C_2 point group were calculated up to the Kohn−Sham ionization threshold. We employed a residual norm of 10^{-5} or less for every eigenpair as convergence criterion. Typically, five or six iterations were required. The Becke-Perdew86 parametrization[38,39] for the exchange-correlation functional was used throughout.

Basis sets have to be chosen with due care for the calculation of response properties. In particular, low-lying virtual orbitals have to be described reasonably well, which is accomplished by polarization functions and, for Rydberg excitations, diffuse functions.

We have performed a series of calibration calculations on naphthalene in order to assess the basis set dependence of the excitation energies and transition moments. SV(P)+ is a standard TURBOMOLE split valence basis set with polarization functions on all atoms except H,[33] augmented with a set of two primitive s, p, and d Gaussians at the center of the naphthalene molecule. (Gaussian orbital exponents: 1s 0.03113631, 1s 0.01532929, 1p 0.01681179, 1p 0.00804768, 1d 0.01258166, 1d 0.00357949.) In this basis, excitation energies are typically 2−3% too small compared with the estimated basis set limit, while oscillator strengths can deviate 20% and more. (Here, of course, we consider only states well below the KS ionization threshold.) This appears sufficient compared to the inherent inaccuracies of the method and the experimental data.

We have also compared the simulated CD spectra of hexahelicene computed with basis sets of different quality. TZVP+ is a TURBOMOLE triple-ζ valence basis with polarization functions on all atoms[40] and additional diffuse augmentation at all ring centers; SV(P)+ contains sets of diffuse functions placed between two rings, respectively. Except for the shoulder at 260 nm (compare Figure 5), which is slightly more pronounced in the larger basis, the SV(P)+ differs from the TZVP+ spectrum only by a small blue shift of 5−10 nm which is almost constant. We note that although the rotatory strengths of individual transitions can deviate considerably, the shape of the entire spectrum is rather insensitive on basis set size.

Table 1. Number of Cartesian Basis Functions N_{bf}, Number of Excitations N_{ex}, and Ionization Thresholds I_{KS} of the Kohn−Sham System (Unshifted)

helicene	N_{bf}	N_{ex}	I_{KS}/nm (eV)
[4]	334	40	231 (5.36)
[5]	418	40	233 (5.33)
[6]	482	40	236 (5.26)
2,15-dicyano-[6]	538	40	212 (5.84)
2,15-dimethoxy-[6]	550	40	236 (5.26)
[7]	546	50	238 (5.20)
[12]	926	80	248 (4.99)

From these investigations it may be concluded that the SV(P)+ basis set is well suited for an effective and sufficiently accurate description of the CD spectra of helicenes in the present context. Consequently, we have chosen it for all calculations reported below. Rotatory strengths were calculated using the dipole-length expression; in most cases, the dipole-velocity form differed by less than 10%. A survey of the number of basis functions, the number of excitations included, and the corresponding KS ionization thresholds is given in Table 1.

C. Simulation of Electronic Circular Dichroism Spectra. The recording of UV−vis spectra in solution is a simple, widely used method for the characterizations of compounds. Normally, one observes broad unresolved bands without fine structure, and the positions as well as the intensities of the peaks can depend considerably on the solvent. An investigation of these details is beyond the scope of the present work. We also neglect contributions arising from zero-point vibration energies, and geometric relaxation effects including vibronic coupling. The latter might be important for some transitions in the observed spectra (see refs 41 and 42 and the discussion in section VI).

For a comparison with experiment it is necessary to make assumptions on the line shape. Empirical studies of Mason et al.[43] have shown that Gaussians centered at the excitation energies and scaled with the calculated rotatory strengths are well suited. For the root mean square width, we always used 0.1 eV. In addition, all spectra were blue-shifted by 0.45 eV; this partly accounts for solvent effects as well as the systematic underestimation of higher excitation energies in TDDFT (compare ref 7 and section VI.C). We stress that this procedure has no rigorous foundation and is merely to aid interpretation of the experimental spectra.

V. Experimental Section

General. IR spectra: Perkin-Elmer FT-IR; ν (cm^{-1}). ^{1}H-NMR and ^{13}C-NMR spectra: Bruker WM 400; δ (ppm) relative to the solvent peak. EI-MS: AEI MS 50; intensities relative to the basis peak. Mp: Reichert apparatus; uncorrected. For enantiomeric separation by HPLC, cellulose-tris(3,5-dimethylphenylcarbamate) (CDMPC) was used. Optical rotations: Perkin-Elmer polarimeter 241; c (g 100 mL^{-1}). CD measurement: Jasco spectropolarimeter J 720.

2,15-Dicyanohexahelicene (1). In a photoreactor equipped with a H_2O-cooled immersion well and a high-pressure Hg lamp a solution of 2,7-bis(*p*-cyanostyryl)naphthalene (382.5 mg, 1 mmol) and iodine (38.1 mg, 0.15 mmol) in toluene (1 L) was irradiated for 3.5 h. Evaporation of the crude product and workup by liquid chromatography (SiO_2: 63−100 μm, cyclohexane/ethyl acetate 1.5:1; $R_f = 0.65$) yielded 234.6 mg (62%) of compound **1**: mp > 300 °C. IR (KBr): ν = 2935 (C−H, aromatic); 2219 (C−N); 1614 (C−C, aromatic). ^{1}H-NMR (400 MHz, $CDCl_3$): δ = 7.44 (d, ^3J = 7.87 Hz, 2H); 7.80 (s, 2H); 7.96−8.13 (m, 10H). ^{13}C-NMR (100.6 MHz, $CDCl_3$): δ = 108.34 (C_q); 118.92 (C_q); 123.64 (C_q); 126.86 (C_q); 127.27 (CH); 128.16 (CH); 128.27 (CH); 128.77 (C_q); 128.79 (CH); 129.62 (CH); 130.16 (CH); 132.58 (C_q); 133.32 (CH); 134.18 (C_q); 134.23 (C_q). MS (EI): m/z = 378.1 (M^+ [$C_{28}H_{14}N_2$], 100); 352.2 (M^+ − CN, 13); 326.2 (M^+ − 2CN,

(38) Becke, A. D. *Phys. Rev. A* **1988**, *36*, 3098.
(39) Perdew, J. P. *Phys. Rev. B* **1986**, *33*, 8822.
(40) Schäfer, A.; Huber, C.; Ahlrichs, R. *J. Chem. Phys.* **1994**, *100*, 5829.
(41) Weigang, O. E., Jr.; Turner, J. A.; Trouard, P. A. *J. Chem. Phys.* **1966**, *45*, 1126.
(42) Weigang, O. E., Jr.; Trouard Dodson, P. A. *J. Chem. Phys.* **1968**, *49*, 4248.
(43) Brown, A.; Kemp, C. M.; Mason, S. F. *J. Chem. Soc. A* **1971**, 751.

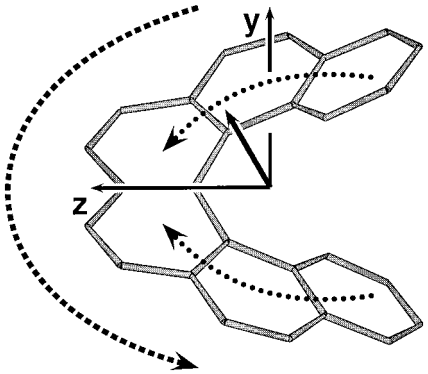

Figure 2. Typical motions of charge induced by electronic transitions of A (dotted lines) and B (dashed line) symmetry.

17); 300.1 ($C_{24}H_{12}^+$, 5). $C_{28}H_{14}N_2$ (378.43). Enantiomeric separation by HPLC. Column: CDMPC, 500 × 4.6 mm. Eluent: *n*-hexane/isopropanol, 9:1, 0.5 mL min^{-1}. Pressure: 3 bar. Temperature: 25 °C. Detection: UV, $\lambda = 254$ nm; t_R [(−)-**1**] = 65.0 min; k'[(−)-**1**] = 3.99; t_R [(+)-**1**] = 80.25 min; k'[(+)-**1**] = 5.16; α =1.29. $[\alpha]_D^{20}$: 3440° ± 400° (c = 0.003, $CHCl_3$).

2,15-Dimethoxyhexahelicene (2). The same method as for **1** was applied to compound **2**,[44] using 2,7-bis(*p*-methoxystyryl)naphthalene (196.3 mg, 0.5 mmol), iodine (19.1 mg, 0.075 mmol), and toluene (1 L). The resulting crude product was chromatographed (SiO_2: 63−100 μm, toluene; $R_f = 0.68$) to give 58.3 mg (30%) of **2**: mp 206 °C. IR (KBr): $\nu = 3000$ (C−H, aromatic); 2955 (C−H, OCH_3); 1607 (C−C, aromatic); 1231 (C−O, OCH_3). ^{1}H-NMR (400 MHz, $CDCl_3$): δ = 3.2 (s, 6H, OCH_3); 7.23 (d, $^3J = 8.68$ Hz, 2H, aromatic); 7.35 (s, 2H, aromatic); 8.06 (d, $^3J = 8.68$ Hz, 2H, aromatic); 8.14 (pt, $^3J = 9.0$ Hz, 4H, aromatic); 8.28 (d, $^3J = 8.18$, 2H, aromatic); 8.32 (d, $^3J = 8.18$, 2H, aromatic). ^{13}C-NMR (100.6 MHz, $CDCl_3$): δ = 54.64 (OCH_3); 107.94 (CH); 118.31 (CH); 124.58 (CH); 127.03 (C_q); 127.40 (CH); 127.52 (CH); 127.61 (CH); 128.59 (C_q); 129.09 (CH); 129.40 (C_q); 131.72 (C_q); 132.18 (C_q); 133.36 (C_q); 157.60 (C_q). MS (EI): m/z = 388.2 (M^+ [$C_{28}H_{20}O_2$], 100); 300.1 ($C_{24}H_{12}^+$, 22). $C_{28}H_{20}O_2$ (388.47). Enantiomeric separation by HPLC. Column: CDMPC, 500 × 4.6 mm. Eluent: *n*-hexane/isopropanol, 99.7:0.3, 2 mL min^{-1}. Pressure: 24 bar. Temperature: 25 °C. Detection: UV, $\lambda = 254$ nm; t_R [(−)-**2**] = 27.0 min; k'[(−)-**2**] = 3.91; t_R. [(+)-**2**] = 39.5 min; k'[(+)-**2**] = 6.18; α = 1.58. $[\alpha]_D^{20}$: 3271.7° ± 7° (c = 0.06, $CHCl_3$).

VI. Results and Discussion

A. General Considerations. The electronic excitations of C_2-symmetric helicenes can be classified according to the two IRs A and B of the point group. We take the *z*-axis as a two-fold symmetry axis, while the helical axis points in the negative *x*-direction. Thus, totally symmetric A transitions are polarized along the *z*-axis, the corresponding transition moments $\boldsymbol{\mu}^{0n}$ and $\mathbf{m}^{0n}$ being parallel to *z*. On the other hand, electric and magnetic transition dipole moments of B-type transitions are orthogonal to *z* leading to a polarization in the *xy*-plane. These constraints imposed by symmetry are an important guide for interpretation and should be remembered in the following discussion.

Figure 2 illustrates typical "motions" of electron charge associated with A and B transitions. The electric transition dipole moment vector $\boldsymbol{\mu}^{0n}$ points in the direction of negative charge movement, eq 8, while the magnetic transition dipole moment, according to eq 11, is a normal vector on the plane of the current $\mathbf{j}^{0n}$ associated with the transition (compare the "right-hand rule" in magnetostatics). It is evident that B transitions take place in the *xy* -plane. Figure 2 also explains why most strong A transitions are almost exclusively found to have positive rotatory strength in left-handed helicenes: The electric and magnetic transition dipole moments are antiparallel, leading to positive rotatory strength according to eq 13. Of course, Figure 2 is only a simplified scheme; in general, nodal planes and changes of sign will occur leading to cancellation or amplification of intensities.

Table 2. TDDFT Results for the Lowest Excitations of (M)-Tetrahelicene Compared to Experiment

	ΔE (nm)			
state	TDDFT[a]	exptl[b]	f	R (10^{-40} cgs)
1 ^{1}B	362 (320)	372	0.001	0.1
1 ^{1}A	353 (313)	328	0.019	19
2 ^{1}A	305 (274)	295	0.043	38
2 ^{1}B	300 (271)	282	0.289	−40
3 ^{1}B	295 (266)	274	0.309	−38

[a] Shifted values in parentheses, as explained in text. [b] Absorption spectrum in pentane.[46]

Previous assignments of electronic excitations in helicenes[41] have often relied on Platt's classification based on free electron states. Application of this simple model to nonplanar helicenes suffers from several shortcomings. Firstly, rigorous σ-π separation is not possible; especially in the strongly distorted terminal rings, π antibonding and σ bonding orbitals are hardly distinguishable. The number of states predicted by the free electron model is therefore too low, especially at shorter wavelength. This is also the case for other π-electron approaches. In addition, the external potential is drastically simplified and correlation is completely neglected, apart from Fermi correlation accounted for by the Aufbau principle. The only virtue of the model, besides its simplicity, is the qualitatively correct nodal structure, which is certainly important for energetic ordering. For example, the symmetry of the lowest excited free electron state is predicted B for helicenes with an even and A for helicenes with an odd number of rings.[41] This is consistent with our calculations and polarized excitation measurements on pentahelicene[43] and hexahelicene.[41,42,45]

B. Tetrahelicene. Tetrahelicene cannot be resolved into enantiomers due to its low racemization barrier (<16 kJ/mol[34]). Some information is available from absorption measurements[46] in solution, compare Table 2, and can be discussed in connection with the calculated CD spectrum (Figure 3).

As expected, the lowest excitation has B symmetry; the rotatory strength is predicted very small. Its calculated excitation energy of 362 nm compares well with the experimental value, 372 nm. Bands A and B in the CD spectrum are due to the lowest two A-type excitations, both with distinctly positive rotatory strength. Our results strongly suggest that the rather weak features observed in the absorption spectrum near 295 nm are caused by the 2 ^{1}A state. The negative band C results from the two close-lying 2 ^{2}B and 3 ^{1}B states. The present calculations are in disagreement with the analysis of Jones and Spinner,[46] who tentatively assign the strong band near 274 nm in their observed spectrum a vibrational progression from 2 ^{1}B.

While, at long wavelength, the spectrum retains some qualitative resemblance with that of hexahelicene, the shorter wavelength part is quite different. Most striking is the lack of positive bands. Features D and E are almost exclusively due to B-type transitions, while the higher A excitations responsible for the large positive bands of the homologues have almost negligible intensities. This is probably due to the comparably small geometric distortion along the *z*-axis. Thus, the structural anomaly of tetrahelicene also shows up in its chiroptical properties.

(44) Brown, J. M.; Field, I. P.; Sidebottom, P. J. *Tetrahedron Lett.* **1981**, *22*, 4867.

(45) Brickell, W. S.; Brown, A.; Kemp, C. M.; Mason, S. F. *J. Chem. Soc. A* **1971**, 756.

(46) Jones, R. N.; Spinner, E. *Spectrochim. Acta* **1960**, *16*, 1060.

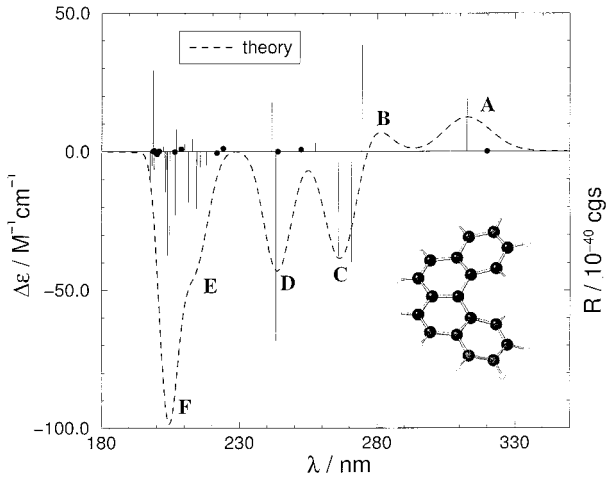

Figure 3. Simulated CD spectrum of (M)-tetrahelicene. The sticks indicate the positions and rotatory strengths of the calculated states. States with very small rotatory strengths are denoted by filled dots. All calculated excitation energies are blue-shifted by 0.45 eV.

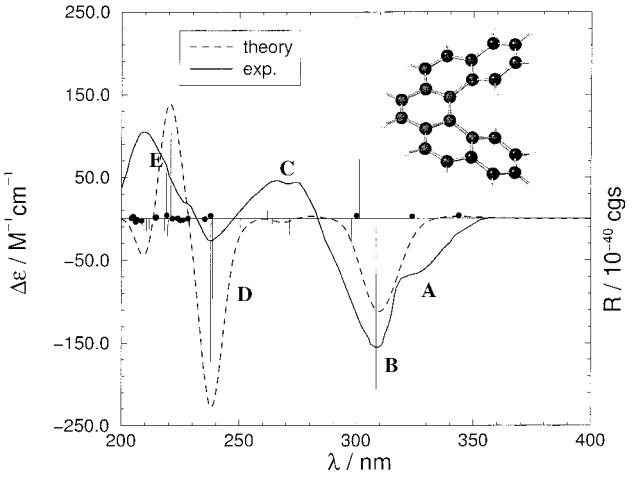

Figure 4. Comparison of simulated and experimental CD spectra of (M)-pentahelicene. The sticks indicate the positions and rotatory strengths of the calculated states. States with very small rotatory strengths are denoted by filled dots. All calculated excitation energies are blue-shifted by 0.45 eV.

Table 3. TDDFT Results for the Lowest Excitations of (M)-Pentahelicene Compared to Experiment

	ΔE (nm)		f		R (10^{-40} cgs)	
state	TDDFT[a]	exptl	TDDFT	exptl[b]	TDDFT	exptl[b]
1 ^{1}A	393 (344)	396,[c] 392[b]	0.001	0.002	3	0.1
1 ^{1}B	367 (324)	344,[c] 328[b]	0.012	0.115	3	−150
2 ^{1}B	347 (309)	310,[c] 306[b]	0.155	0.400	−206	−400
2 ^{1}A	338 (301)		0.042		72	
3 ^{1}A	337 (300)		0.001		3	

[a] Shifted values in parentheses, as explained in text. [b] Absorption spectrum in solution.[43] [c] Matrix isolation spectroscopy data.[47]

C. Pentahelicene. Experimental CD[43] as well as absorption and fluorescence spectra[43,47] have been reported for pentahelicene. The CD spectrum (Figure 4) has a shape similar to that of hexahelicene, which is not unexpected from a structural viewpoint.

In agreement with previous assignments,[43] the lowest three states exhibit A, B, and B symmetry (Table 3). While the TDDFT energy of the first excited singlet state is surprisingly close to experiment, the higher states tend to be too low. This

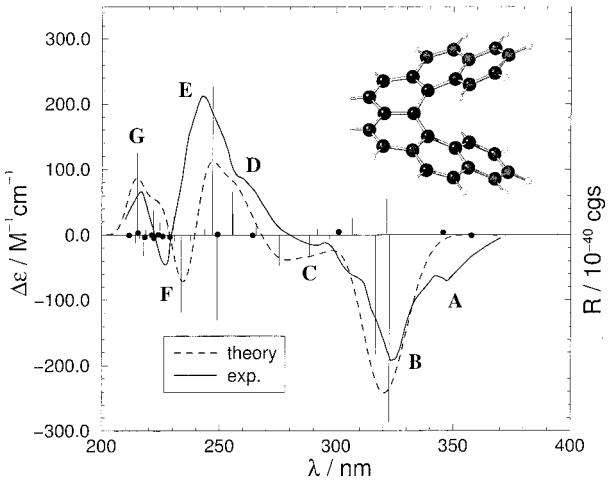

Figure 5. Comparison of simulated and experimental CD spectra of (M)-hexahelicene. The sticks indicate the positions and rotatory strengths of the calculated states. States with very small rotatory strengths are denoted by filled dots. All calculated excitation energies are blue-shifted by 0.45 eV.

pattern is peculiar of TDDFT calculations on aromatic hydrocarbons; it might be related to the fact that the exchange-correlation potential is too flat so that spacings between higher virtual orbitals are too small. The calculated rotatory strength of the 1 ^{1}B transition is nearly zero, in contrast to the pronounced shoulder A in the experimental spectrum. A similar phenomenon is observed in the 1 ^{1}A state of hexahelicene and its derivatives. Whether the method fails here or vibronic coupling may change intensities considerably cannot be decided at this stage. However, we also note significant differences between the absorption measurements in solution and the probably more accurate matrix isolation data for this excitation. The strongly negative band B dominates the low-energy part of the spectrum; it emerges from the 2 ^{1}B transition. According to our calculations, the neighboring 2 ^{1}A states are responsible for the additional peak in the absorption spectrum near 300 nm, while their total contribution to CD is small. Structure C results from several states with different character and can certainly not be explained by a single state, as suggested by Brown, Kemp, and Mason.[43] Calculated intensities are too small,while for bands D and E they are clearly too large, but of correct sign (band E might be incomplete because of the onset of the KS continuum).

D. Hexahelicene. Hexahelicene is the paradigm of the helically chiral molecule. Its absorption and CD spectra have been the object of repeated experimental studies.[41,42,45,48] The CD spectrum of the left-handed enantiomer (Figure 5) shows the characteristic strongly negative band at long wavelength determining the rotatory dispersion in the visible, while positive absorption is found at shorter wavelength. Our calculations predict the low-energy bands to arise from transitions polarized in the *xy*-plane (B symmetry), while the positive high-energy bands are mainly caused by A-type transitions polarized along the *z*-axis. This agrees well with polarized absorption measurements on hexahelicene.[41,42,45]

The lowest excited state of hexahelicene has B symmetry (Table 4); its nearly zero rotatory strength results from large *x* and *y* contributions which almost cancel. Under these circumstances, the predicted sign has little significance. The transition frequency is again accurately reproduced by the calculations. The 1 ^{1}A excitation is predicted too low and with small

(47) Palewska, K.; Chojnacki, H. *Mol. Cryst. Liq. Cryst.* **1993**, *229*, 31.

(48) Newman, M. S.; Darlak, R. S.; Tsai, L. *J. Am. Chem. Soc.* **1967**, *89*, 6191.

Table 4. TDDFT Results for the Lowest Excitations of (M)-Hexahelicene Compared to Experiment

	ΔE (nm)		f		R (10^{-40} cgs)	
state	TDDFT[a]	exptl	TDDFT	exptl[b]	TDDFT	exptl[b]
1 ^{1}B	411 (358)	411,[c] 412[b]	0.003	0.002	−1	1.6
1 ^{1}A	395 (346)	351,[c] 347[b]	0.002	0.043	4	−86
2 ^{1}B	365 (323)	326,[c] 325[b]	0.168	0.492	−287	−247
2 ^{1}A	364 (321)		0.025		55	
3 ^{1}B	358 (316)	314[c]	0.066		−183	

[a] Shifted values in parentheses, as explained in text. [b] Absorption spectrum in solution,[45] sign of R inverted. [c] Absorption spectrum in solution.[42]

intensities, similar to the situation encountered for the 1 ^{1}B state of pentahelicene. Further, the calculations reveal that band B, commonly attributed to the 2 ^{1}B state, results from three close-lying states, 2 ^{1}B, 2 ^{1}A (with moderately positive intensity), and 3 ^{1}B. This agrees with the additional structure observed in the absorption spectrum[45] near 330 nm. An analysis of the orbital contributions according to eq 16 shows that 1 ^{1}B and 2 ^{1}B are strongly related as they both consist mainly of the same two single-particle transitions describing motions of charge along the helical axis, compare Figure 2. The individual contributions cancel in 1 ^{1}B, while they sum up to a large negative rotatory strength in 2 ^{1}B. The strongly positive band E near 250 nm is not simply due to a single transition as proposed by Brown, Kemp, and Mason; instead, it results from an intricate cancellation between the 9 ^{1}A ($R = 227$ cgs) and the 9 ^{1}B ($R = -131$ cgs) states. Shoulder D arises from the very close 7 ^{1}A and 8 ^{1}B transitions, both with positive calculated rotatory strength. This complex interplay is described quite satisfactorily by TDDFT. The terminal rings obviously are important for the strong A-type transitions not present in the smaller helicenes. The short-wavelength region between 200 and 250 nm is characterized by numerous states with small intensities. Despite the increasing red-shift and a spuriously large positive band near 220 nm, the calculations are still in qualitative agreement with experiment.

E. 2,15-Disubstituted Hexahelicenes. Experimental CD spectra of 2,15-dicyanohexahelicene and 2,15-dimethoxyhexahelicene have been recorded for the present work and are presented here for the first time (Figures 6 and 7).

A characteristic feature is the overall red-shift of the observed spectra compared to hexahelicene; it is most pronounced for the dicyano compound. This phenomenon may be attributed to an enlargement of the π-electron system and is reproduced by the calculations. For example, the predicted shifts of band B (0.12 and 0.08 eV for the dicyano and dimethoxy compounds) agree rather well with experiment (0.19 and 0.12 eV). The long-wavelength region of the spectra resembles that of hexahelicene otherwise. This changes below 300 nm, where quite characteristic patterns for different substituents are found. In the dicyano compound, intensification of the 6 ^{1}A transition produces the distinct band D. The same is true for band G arising from 16 ^{1}A; its rotatory strength is drastically overestimated by TDDFT. In the dimethoxy derivate, additional states occur leading to bands D and E, while small total intensities are found near 290 nm (C). D and E are not resolved in the simulation, partly because the underlying transitions 11 ^{1}A and 12 ^{1}A are predicted too close, and partly because of the simulation scheme which assumes constant line width. Band G lies above the KS continuum and therefore is beyond the present scope of TDDFT. Although agreement with experiment is not perfect, it is certainly sufficient for identification of the derivates and assignment of the dominant transitions.

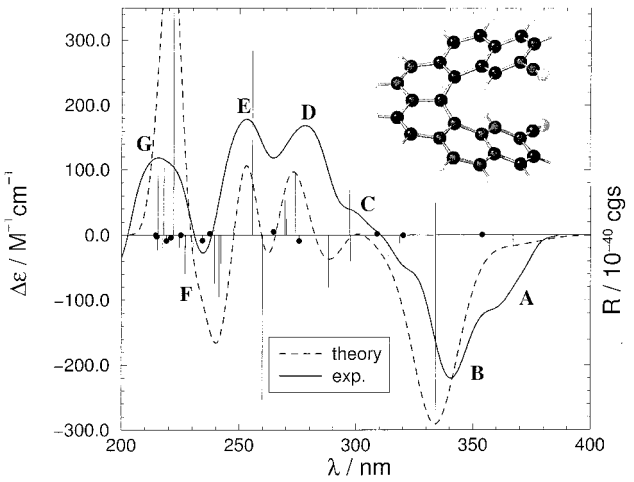

Figure 6. Comparison of simulated and experimental CD spectra of (M)-2,15-dicyanohexahelicene. The sticks indicate the positions and rotatory strengths of the calculated states. States with very small rotatory strengths are denoted by filled dots. All calculated excitation energies are blue-shifted by 0.45 eV.

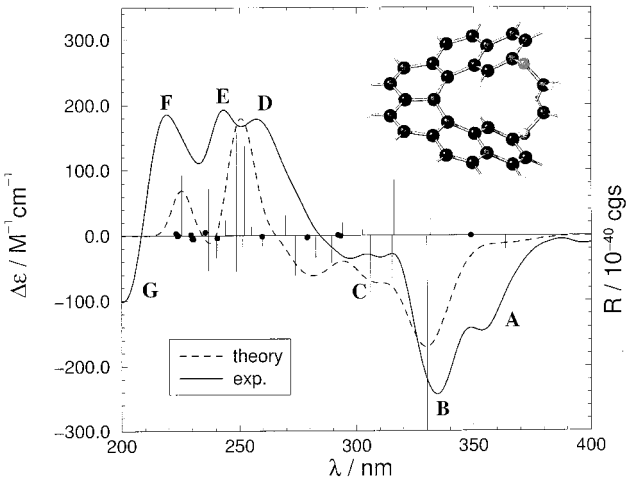

Figure 7. Comparison of simulated and experimental CD spectra of (M)-2,15-dimethoxyhexahelicene. The sticks indicate the positions and rotatory strengths of the calculated states. States with very small rotatory strengths are denoted by filled dots. All calculated excitation energies are blue-shifted by 0.45 eV.

F. Heptahelicene. Experimental CD[45] as well as absorption spectra[45,47] are available for this compound. However, the quality of the data is poor and detailed comparison with theory (Figure 8, Table 5) is hampered by low resolution.

The first excited singlet state, 1 ^{1}A, is omitted by Brown, Kemp, and Mason[45] but found in the absorption spectrum.[47] Its rotatory strength is very small, as in the lower homologues. The 1 ^{1}B excitation is weak and very close to the strongly negative 2 ^{1}B; not surprisingly, it has not yet been observed. Compared to hexahelicene, the splitting between 2 ^{1}B and 3 ^{1}B is larger and the latter transition gains intensity, leading to considerable broadening of band A. In the short-wavelength region, the spectrum resembles rather that of pentahelicene. Feature B near 300 nm is predicted a large negative band by TDDFT while the experimental data only show a plateau on a steeply rising positive background. A similar picture emerges for pentahelicene; in both cases, rotatory strengths of the 6 ^{1}B and 7 ^{1}B states are probably overestimated by the calculations, although this cannot be definitely judged unless vibronic effects are accounted for. Band C is analogous to band E of pentahelicene,

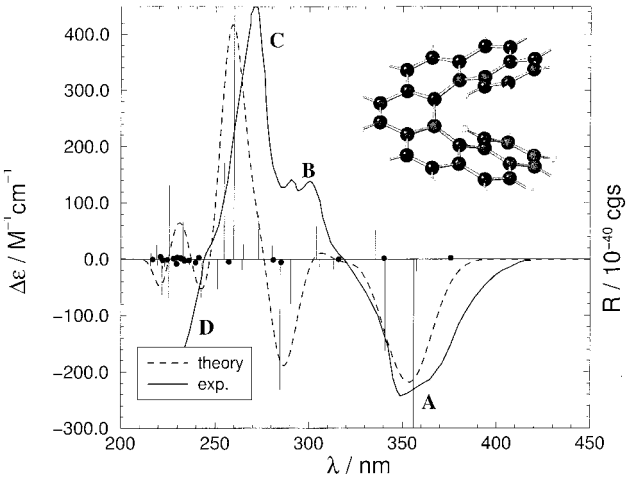

Figure 8. Comparison of simulated and experimental CD spectra of (M)-heptahelicene. The sticks indicate the positions and rotatory strengths of the calculated states. States with very small rotatory strengths are denoted by filled dots. All calculated excitation energies are blue-shifted by 0.45 eV.

Table 5. TDDFT Results for the Lowest Excitations of (M)-Heptahelicene Compared to Experiment

	ΔE (nm)		f		R (10^{-40} cgs)	
state	TDDFT[a]	exptl	TDDFT	exptl[b]	TDDFT	exptl[b]
1 ^{1}A	435 (376)	422[c]	0.001		2	
1 ^{1}B	411 (357)		0.005		−22	
2 ^{1}B	409 (356)	386[c]	0.035		−303	
3 ^{1}B	389 (341)	347,[d] 364[e]	0.061	0.370	−162	−250
2 ^{1}A	388 (340)		0.002		1	
3 ^{1}A	382 (335)		0.022		51	

[a] Shifted values in parentheses, as explained in text. [b] Absorption spectrum in solution.[45] [c] Matrix isolation spectroscopy data.[47] [d] Absorption spectrum in ethanol, 298 K.[47] [e] Reference 45, maximum of the CD spectrum.

but its intensity is greatly increased. This is qualitatively well reproduced by TDDFT, despite a small unexpected blue-shift. Band C is found to originate from A transitions along the *z*-axis with considerable contributions from the terminal rings.

G. Dodecahelicene. Dodecahelicene is the largest member of the helicene family treated in the present work. Experimental spectra are unknown, but, considering the smaller cases, we are optimistic that our simulation (Figure 9) has some predictive value. Due to its dimensions and the relatively large density of states, dodecahelicene also can serve as a benchmark for our implementation.

As in hexahelicene, the lowest excited state has B symmetry and nearly vanishing rotatory strength ($R = -4$ cgs). Band A is reminiscent of the B band in hexahelicene; the two strongly negative peaks are caused by 2 ^{1}B and 3 ^{1}B. However, note the appreciable red-shift compared to the smaller compound. From the negative sign of A one may conclude that the left-handed enantiomer has negative specific rotation in the visible. Near 340 nm, a new band B occurs, mainly caused by 9 ^{1}B and 10 ^{1}B. Similarly, at shorter wavelength, we find two positive bands D and F instead of a single one in hexahelicene, separated by the small negative feature E. The latter is remarkable because it is caused by an A-type transition. With increasing level

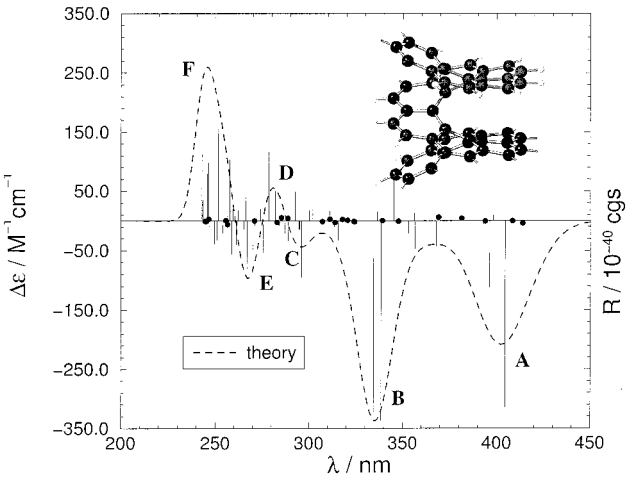

Figure 9. Simulated CD spectrum of (M)-dodecahelicene. The sticks indicate the positions and rotatory strengths of the calculated states. States with very small rotatory strengths are denoted by filled dots. All calculated excitation energies are blue-shifted by 0.45 eV.

density, assignments of individual states become more and more meaningless. We can still say that bands D and F have predominantly A character. Compared to the lower homologues, absolute band intensities increase only moderately.

VII. Conclusions

The CD spectra of (M)-[*n*]helicenes, $n = 4-7$, 12, are roughly characterized by B-type transitions with negative rotatory strengths at long wavelength and, apart from tetrahelicene, positive bands at shorter wavelength mainly caused by transitions of A symmetry. For hexahelicene, the latter region is found particularly sensitive to substituents in the terminal rings. The lowest excited state has almost vanishing rotatory strength and alternating symmetry (with ring numer *n*). General trends are an increasing overall red-shift and enhancement of band intensities with increasing number of rings. In many respects, tetrahelicene is an exception; this is clearly related to its structural anomaly.

TDDFT is a prime tool for investigations on molecular chiroptical properties. It combines moderate accuracy with low computational cost and provides a simple intuitive interpretation. Improvements in accuracy would be desirable, but in several cases we feel that a proper treatment of vibrational and solvation effects might be important, too. Unless one introduces additional empirical parameters and other approximations, the inherent shortcomings of the method are, to some extent, under control. Within these limitations, TDDFT can be expected to give a reliable description of circular dichroism in many realistic chemical systems.

Acknowledgment. This work was supported by the Deutsche Forschungsgesellschaft, SFB 195 ("Lokalisierung von Elektronen in makroskopischen und mikroskopischen Systemen") and SFB 332 ("Wechselwirkungen in Molekülen").

Supporting Information Available: HF-optimized atomic coordinates, calculated excitation energies, and transition strengths for all compounds (ASCII). This material is available free of charge via the Internet at http://pubs.acs.org.

JA991960S